Faraday Discussions

Cite this: *Faraday Discuss.*, 2022, **234**, 34

ROYAL SOCIETY OF CHEMISTRY

PAPER

View Article Online
View Journal | View Issue

A bio-inspired heterodinuclear hydrogenase CoFe complex†

Lili Sun,‡[a] Suzanne M. Adam,‡[ab] Walaa Mokdad,[a] Rolf David,[a] Anne Milet,[a] Vincent Artero *[b] and Carole Duboc *[a]

Received 8th November 2021, Accepted 2nd December 2021
DOI: 10.1039/d1fd00085c

Herein, a new heterobimetallic CoFe complex is reported with the aim of comparing its performance in terms of H_2 production within a series of related MFe complexes (M = Ni, Fe). The fully oxidized $[(L^{N2S2})Co^{II}(CO)Fe^{II}Cp]^+$ complex (**$Co^{II}Fe^{II}$**, $L^{N2S2\ 2-}$ = 2,2′-(2,2′-bipyridine-6,6′-diyl)bis(1,1′-diphenylethanethiolate), Cp^- = cyclopentadienyl anion) can be (electro)chemically reduced to its **$Co^{I}Fe^{II}$** form, and both complexes have been isolated and fully characterized by means of classic spectroscopic techniques and theoretical calculations. The redox properties of **$Co^{II}Fe^{II}$** have been investigated in DMF, revealing that this complex is the easiest to reduce by one-electron among the analogous MFe complexes (M = Ni, Fe, Co). Nevertheless, it displays no electrocatalytic activity for H_2 production, contrary to the FeFe and NiFe analogs, which have proven remarkable performance.

Introduction

Hydrogenases are metalloenzymes present in certain organisms – bacteria or microalgae – which have the capacity to produce or oxidize hydrogen.[1–4] Remarkably, they reversibly catalyze the conversion of protons into molecular hydrogen at a potential close to the thermodynamic potential ($E^0_{app}(H^+/H_2) = -413$ mV in water at pH 7 and 25 °C under 0.1 bar of H_2). Two main classes of hydrogenases are known, differing by the nature of their active sites. The active site of the [NiFe]-hydrogenases consists of a heterodinuclear NiFe complex, where the two metal ions are bridged by thiolate moieties from the cysteine residues of the polypeptide chain. In the case of the [FeFe]-hydrogenases, the active site is a dinuclear iron complex with the two Fe ions also connected by two thiolate functionalities, but arising from an unusual ligand in biology, *i.e.*, dithiomethylamine. These two organometallic MFe clusters (M = Ni or Fe) present a unique structure in biology with the presence of carbon monoxide (CO) and

[a]*Univ. Grenoble Alpes, CNRS UMR 5250, DCM, F-38000 Grenoble, France. E-mail: carole.duboc@univ-grenoble-alpes.fr*
[b]*Univ. Grenoble Alpes, CNRS, CEA, Laboratoire de Chimie et Biologie des Métaux, F-38000 Grenoble, France*
† Electronic supplementary information (ESI) available. See DOI: 10.1039/d1fd00085c
‡ Equal contribution of the co-authors.

cyanide (CN^-) as iron ligands. These structures contribute to these systems' unique electronic properties, which facilitate the protonation of the metal sites under mild conditions, thereby making hydrogenases great catalysts for H_2 production. Thus, mimicking the activity of these enzymes with bio-inspired complexes to develop new catalysts for H_2 production has quickly emerged as an attractive strategy for chemists.[5–8]

Recently, we described the H_2 production reactivity of two dinuclear $M^{II}Fe^{II}$ (M = Fe or Ni) complexes with similar structures. We have demonstrated that both $[(L^{N2S2})Ni^{II}Fe^{II}Cp(CO)]^+$ (**$Ni^{II}Fe^{II}$**)[9,10] and $[(L^{N2S2})(MeCN)Fe^{II}(CO)Fe^{II}Cp]^+$ (**$Fe^{II}Fe^{II}$**)[11,12] complexes (L^{N2S2}: 2,2′-(2,2′-bipyridine-6,6′-diyl)bis(1,1′-diphenylethanethiolate), Cp = cyclopentadienyl, Scheme 1) display comparable electrocatalytic performance for H_2 production, both following an *E*[ECEC] catalytic mechanism (E = electron transfer, C = chemical reaction, *e.g.*, a protonation step in the present case). This absence of notable changes in the reactivity was rationalized by the non-innocent redox activity of the L^{N2S2} ligand that is proposed to dominate the catalytic process.[13] Since it has been shown that Co complexes can display high performance for H_2 production,[14–17] we describe herein the investigation of the **$Co^{II}Fe^{II}$** parent complex, with the aim of comparing its reactivity with its NiFe and FeFe analogs. The target $[(L^{N2S2})Co^{II}(CO)Fe^{II}Cp]^+$ complex, **$Co^{II}Fe^{II}$**, has been synthesized and characterized, and its reduction chemistry as well as its H_2 production reactivity have been investigated.

Results and discussion

Synthesis and characterization of $Co^{II}Fe^{II}$

An equimolar mixture of $[Co^{II}(L^{N2S2})]$ and $[Fe^{II}(CO)(Cp)(CH_3CN)_2]BF_4$ stirred overnight in dichloromethane (DCM) at room temperature under an inert atmosphere affords the dark brown $[(L^{N2S2})Co^{II}(CO)Fe^{II}(Cp)]BF_4$ target complex

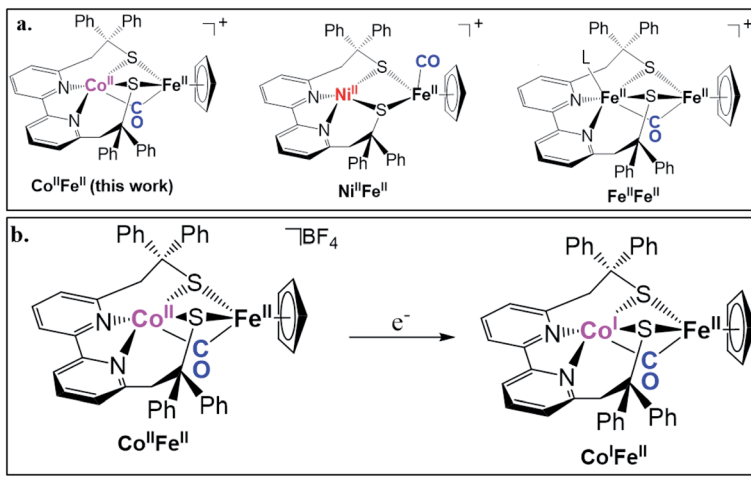

Scheme 1 (a) Family of dinuclear model complexes (CoFe (this work), NiFe,[11] and FeFe,[10] with L = CO or solvent). (b) Reduction reactivity of the **$Co^{II}Fe^{II}$** complex described in this work.

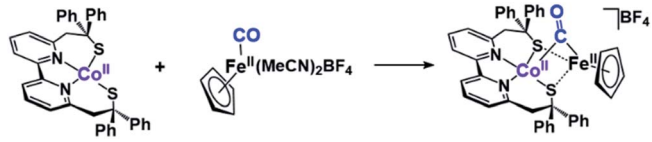

Scheme 2 Synthetic pathway to afford $Co^{II}Fe^{II}$.

($\mathbf{Co^{II}Fe^{II}}$), which could be isolated with high yield (Scheme 2). The optical spectrum of a solution of $\mathbf{Co^{II}Fe^{II}}$ in dimethylformamide (DMF) displays two features in the visible region of the spectrum with $\lambda_{max} = 468$ nm ($\varepsilon = 4900\ M^{-1}\ cm^{-1}$) and 584 nm ($\varepsilon = 3100\ M^{-1}\ cm^{-1}$), distinct from the spectra of the mononuclear reagents (see Fig. S1†). The ESI mass spectrum supports the overall formulation, $[(L^{N2S2})Co^{II}Fe^{II}(CO)(Cp)]^+$, with the major mass peak being observed at m/z = 786.04 (calc. 786.09).

Infrared spectroscopy was employed to monitor the binding mode of the CO moiety in $\mathbf{Co^{II}Fe^{II}}$. A stretching frequency is observed at 1856 cm^{-1} in the range

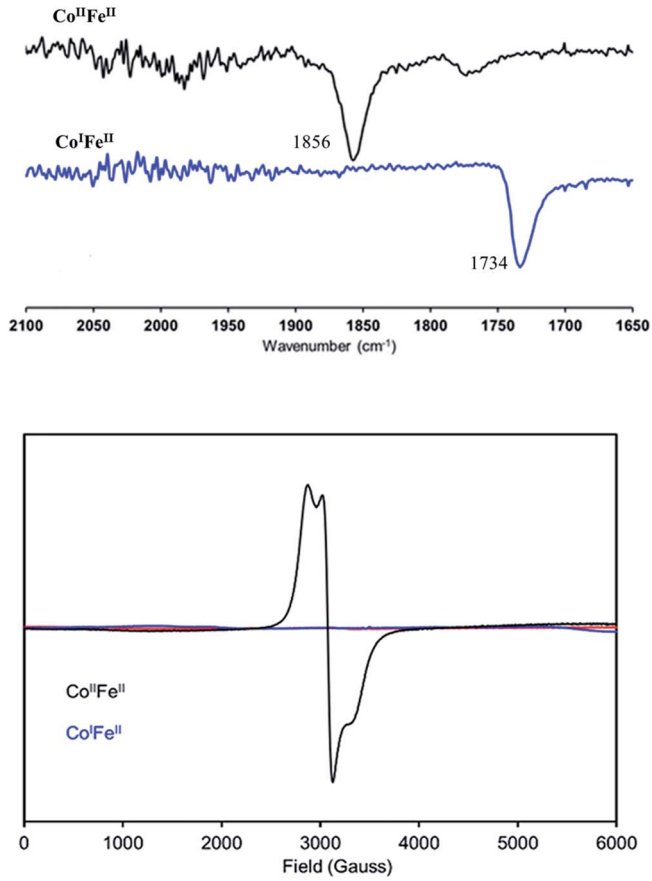

Fig. 1 Attenuated total reflectance infrared (top) and 100 K solid-state EPR (bottom) spectra of $Co^{II}Fe^{II}$ (black) and $Co^{I}Fe^{II}$ (blue) complexes.

for metal-bridging CO moieties (Fig. 1), at an energy close to that found in the $\mathbf{Fe^{II}Fe^{II}}$ derivative (1822 cm^{-1}), and at a significantly lower energy than the terminal M–CO stretching frequencies present in the $[Fe^{II}(CH_3CN)_2(CO)(Cp)]BF_4$ reagent[18] and the analogous $\mathbf{Ni^{II}Fe^{II}}$ complex[9] (1984 and 1929 cm^{-1}, respectively). Based on these data, it can be concluded that the CO bridges the Co^{II} and Fe^{II} ions in $\mathbf{Co^{II}Fe^{II}}$, both in solution (see Fig. S2†) and in the solid state (Fig. 1, bottom).

In order to gain insight into the electronic structure of this heterodinuclear complex, EPR spectra were recorded both as a powder sample (Fig. 1) and as a frozen DMF solution (Fig. S2†) sample at 100 K. The solid-state sample clearly shows a rhombic spectrum ($g_x = 2.24$; $g_y = 2.09$; $g_z = 1.98$) consistent with a low-spin d^7 Co^{II} species. In this case, the d^6 Fe^{II} center does not contribute to the spectrum indicating that the single unpaired electron of the overall $S = \frac{1}{2}$ complex is localized on the Co center. A hyperfine interaction ($I = 7/2$ for ^{59}Co) is resolved in the frozen DMF solution sample spectrum, supporting the Co^{II} assignment (see ESI, Fig. S2†).

To further investigate the structural and spectroscopic properties of $\mathbf{Co^{II}Fe^{II}}$, DFT calculations were carried out. Its optimized structure, $\mathbf{Co^{II}Fe^{II}}$*, displays predicted spectroscopic parameters consistent with the experimental ones, especially regarding the calculated ν_{CO} vibration at 1887 cm^{-1} (*vs.* ν_{CO} exp. at 1856 cm^{-1}). The overall spin state of the complex is confirmed to be a doublet (the quartet is predicted to be at a much higher energy, see Table S1†). The Mulliken spin population of 1.1 on the Co ion is fully consistent with a localized $S = \frac{1}{2}$ $\mathbf{Co^{II}Fe^{II}}$ complex, as proposed by the experimental EPR data (see Fig. S3† for the spin density).

Redox properties of $Co^{II}Fe^{II}$

The cyclic voltammogram (CV) of a DMF solution of $\mathbf{Co^{II}Fe^{II}}$ reveals two diffused-controlled (quasi-)reversible one-electron processes, centered at $E_{1/2} = -1.00$ V ($\Delta E_p = 100$ mV) and $E_{1/2} = -2.04$ V ($\Delta E_p = 80$ mV) *vs.* $Fc^{+/0}$ (Fig. 2). The redox system at −1.00 V can be attributed to the $Co^{II/I}$ reduction, and that at more negative potential, to the reduction of the redox-non-innocent bipyridine ligand. The $Co^{II/I}$ reduction potential against ferrocene, obtained *via* DFT (see ESI for details and Table S2†) is in perfect agreement with a value of −1.02 V *vs.* $Fc^{+/0}$.

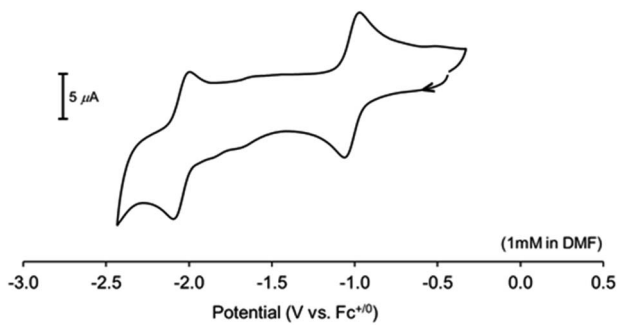

Fig. 2 Cyclic voltammogram of a DMF solution of $\mathbf{Co^{II}Fe^{II}}$ (1 mM); electrolyte: 0.1 M $(Bu)_4NClO_4$; reference: $Ag/AgNO_3$; counter: Pt wire; scan rate: 100 mV s^{-1}.

Such assignments can be proposed based on the comparison of its redox properties to those of the analogous $\mathbf{Fe^{II}Fe^{II}}$ and $\mathbf{Ni^{II}Fe^{II}}$ complexes.[9,11] The CV of $\mathbf{Ni^{II}Fe^{II}}$ reported in MeCN shows two reversible redox systems at −1.29 V and −1.90 V *vs.* $Fc^{+/0}$, attributed to the $Ni^{II/I}$ and L^{N2S2} reduction processes, respectively. The reduction of the Ni^{II} ion in $\mathbf{Ni^{II}Fe^{II}}$ occurs at a significantly more positive potential than in the mononuclear $[Ni^{II}(L^{N2S2})]$ complex under the same conditions ($E_{1/2} = -1.82$ V *vs.* $Fc^{+/0}$ corresponding to a potential shift of 530 mV), highlighting the strong electronic effect of the Lewis acidic Fe component. The $Co^{II/I}$ reduction potential in $\mathbf{Co^{II}Fe^{II}}$ is shifted to an even greater extent (700 mV) as compared to the mononuclear $[Co^{II}(L^{N2S2})]$, which displays a quasi-reversible $Co^{II/I}$ wave at −1.7 V *vs.* $Fc^{+/0}$ in DMF.[14] Regarding $\mathbf{Fe^{II}Fe^{II}}$, the diiron analog exists as the mono-CO form in acetonitrile at a concentration of 0.2 mM, with a bridging CO ligand similar to that found in $\mathbf{Co^{II}Fe^{II}}$ (see Scheme 1). Under these conditions, the first one-electron reduction process occurs at −1.21 V *vs.* $Fc^{+/0}$ resulting in the delocalized, mixed-valent $Fe^{1.5}Fe^{1.5}$ species. In this series of $M^{II}Fe^{II}$ complexes, $\mathbf{Co^{II}Fe^{II}}$ is, therefore, the easiest to reduce.

In the analogous $\mathbf{Fe^{II}Fe^{II}}$ and $\mathbf{Ni^{II}Fe^{II}}$ complexes, it was shown that the second one-electron reduction process occurs at the bipyridine moiety of the L^{N2S2} ligand, at $E_{1/2} = -1.65$ V and $E_{1/2} = -1.90$ V *vs.* $Fc^{+/0}$, respectively, in MeCN. In the case of $\mathbf{Co^{II}Fe^{II}}$, the redox system associated with the bipyridine ligand occurs at a less negative potential, $E_{1/2} = -2.04$ V *vs.* $Fc^{+/0}$ in DMF. The small difference with $\mathbf{Ni^{II}Fe^{II}}$ can be explained by the difference in the solvent (DMF *vs.* acetonitrile), while that with $\mathbf{Fe^{II}Fe^{II}}$ likely arises from differences in the structural and electronic properties of the one-electron reduced species (see below).

Synthesis and characterization of the one-electron reduced $Co^{I}Fe^{II}$ species

The $\mathbf{Co^{II}Fe^{II}}$ complex can be chemically reduced using one molar equiv. of cobaltocene ($CoCp_2$), to generate the one-electron reduced species $\mathbf{Co^{I}Fe^{II}}$ (see ESI‡ for details). Based on the electrochemical analysis, it has been proposed that the reduction occurs at the cobalt center. This conclusion is experimentally supported by the disappearance of the X-band EPR feature present in the

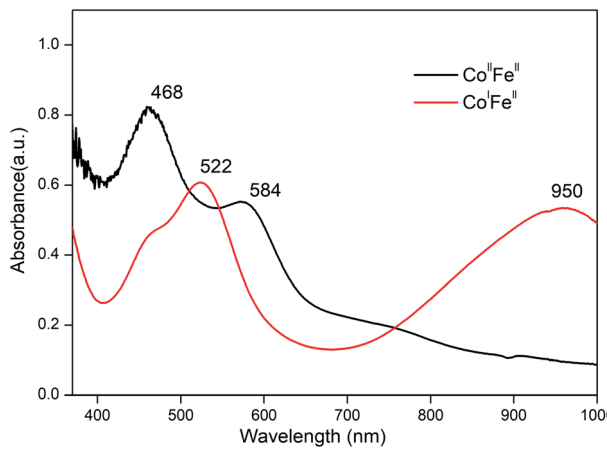

Fig. 3 UV-visible spectra of the $Co^{II}Fe^{II}$ (black), $Co^{I}Fe^{II}$ (red) complexes (0.1 mM, DMF).

spectrum of $\mathbf{Co^{II}Fe^{II}}$ (Fig. 1). The EPR-silent spectrum of $\mathbf{Co^{I}Fe^{II}}$ thus confirms an overall $S = 0$ complex (Co^{I}, d^8; Fe^{II}, d^6). The IR spectrum displays a CO vibrational frequency at 1734 cm^{-1} consistent with a bridging mode (Fig. 1). With respect to $\mathbf{Co^{II}Fe^{II}}$ (1856 cm^{-1}) the energy of this vibration is notably weaker, indicating an elongation of the bridging C═O bond. Distinct changes in the optical profile are also observed upon reduction (Fig. 3), including the growth of a broad, low-energy d–d transition feature (950 nm; $\varepsilon = 1500\ M^{-1}\ cm^{-1}$).

The structural and spectroscopic properties of $\mathbf{Co^{I}Fe^{II}}$ have been further investigated by DFT calculations. The predicted CO vibration calculated from its optimized structure, $\mathbf{Co^{I}Fe^{II}}$*, is consistent with the experimental ones, *i.e.*, ν_{CO}

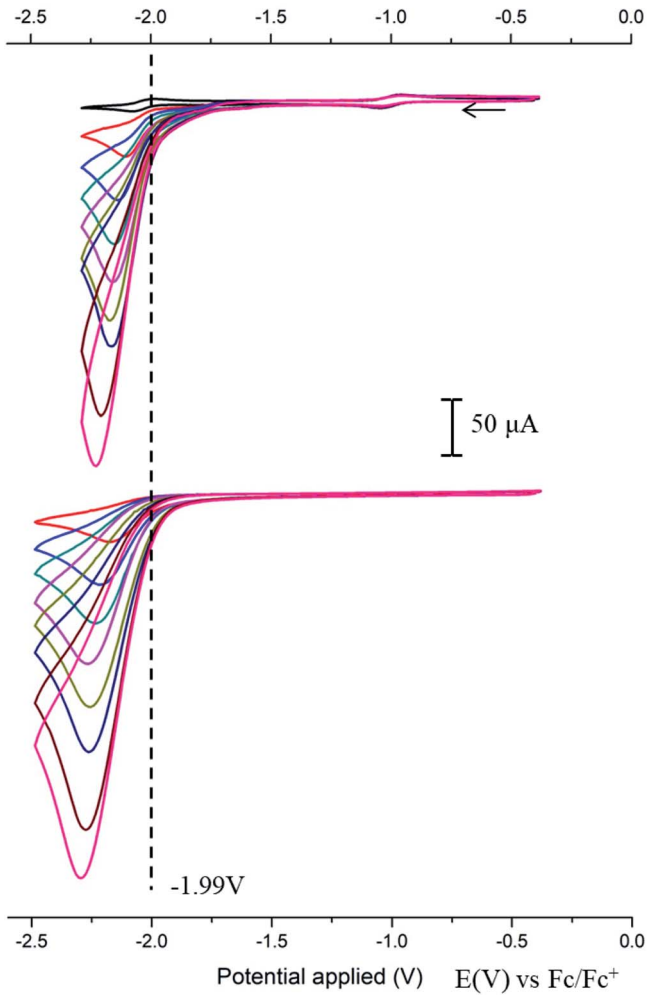

Fig. 4 Top: CVs of $\mathbf{Co^{II}Fe^{II}}$ (0.73 mM, top, black) in the absence or presence of various amounts of Et_3NHBF_4 in DMF solution, 0.1 M *n*-Bu_4NClO_4, on a glassy carbon electrode at 100 mV s^{-1}: 5 equiv. (red); 10 equiv. (blue); 15 equiv. (cyan); 20 equiv. (pink); 25 equiv. (dark yellow); 30 equiv. (dark blue); 40 equiv. (deep red); 50 equiv. (magenta). Bottom: CVs of the corresponding blank samples (no catalyst).

vibration at 1779 cm^{-1} *vs.* ν_{CO} exp. at 1734 cm^{-1}. The overall spin state of the complex is confirmed to be a singlet in agreement with the EPR-silent spectrum.

Reactivity of $Co^{II}Fe^{II}$ in the presence of H^+

Following the addition of Et_3NHBF_4 as a proton source, a catalytic process (E_{cat} = −1.99 V *vs.* Fc/Fc^+, measured at the mid wave at a concentration of 10.95 mM of Et_3NHBF_4) develops on top of the second wave of the $\mathbf{Co^{II}Fe^{II}}$ complex (Fig. 4). Nevertheless, when compared with the CVs recorded under the same conditions, but in the absence of $\mathbf{Co^{II}Fe^{II}}$, the reduction appears to occur at a similar potential evidencing that the presence of $\mathbf{Co^{II}Fe^{II}}$ has a marginal impact, if any, on the H_2 production catalyzed by the glassy carbon surface of the electrode. This electrochemical behavior was completely unexpected since the investigation of both $\mathbf{Ni^{II}Fe^{II}}$ and $\mathbf{Fe^{II}Fe^{II}}$ supported the fact that the nature of the metal bound by the L^{N2S2} ligand has no notable impact on the performance of these electrocatalysts, and that the bipyridine unit was the key factor in controlling their reactivity.[11]

Conclusions

The target $\mathbf{Co^{II}Fe^{II}}$ complex was synthesized with the aim of comparing its reactivity towards H_2 production with its NiFe and FeFe analogs. We were also able to isolate and characterize the corresponding one-electron reduced species. Unexpectedly, this new complex was not active to produce H_2 electrocatalytically, while the analogous NiFe and FeFe complexes have demonstrated remarkable performance. Current work in our laboratories focuses on understanding the origin of this lack of reactivity, since $\mathbf{Co^{II}Fe^{II}}$ displays the most promising redox properties, *i.e.*, it is the easiest to reduce within the series of $M^{II}Fe^{II}$ complexes.

Conflicts of interest

There are no conflicts to declare.

Acknowledgements

Financial support for this work was provided by the Agence National de la Recherche in the framework of the "Investissements d'avenir" Program (ANR-15-IDEX-02), the Labex ARCANE (ANR-11-LABX-003), and the CBH-EUR-GS (ANR-17-EURE-0003), and ANR-DFG (ANR-16-CE92_0012_01 NiFeMim) and by the China Scholarship Council.

References

1 W. Lubitz, H. Ogata, O. Rüdiger and E. Reijerse, *Chem. Rev.*, 2014, **114**, 4081–4148.
2 D. Schilter, J. M. Camara, M. T. Huynh, S. Hammes-Schiffer and T. B. Rauchfuss, *Chem. Rev.*, 2016, **116**, 8693–8749.
3 Y. Nicolet, C. Piras, P. Legrand, C. E. Hatchikian and J. C. Fontecilla-Camps, *Structure*, 1999, **7**, 13–23.
4 A. Volbeda, M.-H. Charon, C. Piras, E. C. Hatchikian, M. Frey and J. C. Fontecilla-Camps, *Nature*, 1995, **373**, 580–587.

5 S. Kaur-Ghumaan and M. Stein, *Dalton Trans.*, 2014, **43**, 9392–9405.
6 A. C. Ghosh, C. Duboc and M. Gennari, *Coord. Chem. Rev.*, 2021, **428**, 213606.
7 N. Coutard, N. Kaeffer and V. Artero, *Chem. Commun.*, 2016, **52**, 13728–13748.
8 J. T. Kleinhaus, F. Wittkamp, S. Yadav, D. Siegmund and U.-P. Apfel, *Chem. Soc. Rev.*, 2021, **50**, 1668–1784.
9 D. Brazzolotto, M. Gennari, N. Queyriaux, T. R. Simmons, J. Pécaut, S. Demeshko, F. Meyer, M. Orio, V. Artero and C. Duboc, *Nat. Chem.*, 2016, **8**, 1054–1060.
10 M. E. Ahmed, S. Chattopadhyay, L. K. Wang, D. Brazzolotto, D. Pramanik, D. Aldakov, J. Fize, A. Morozan, M. Gennari, C. Duboc, A. Dey and V. Artero, *Angew. Chem., Int. Ed.*, 2018, **57**, 16001–16004.
11 L. Wang, M. Gennari, A. Barrozo, J. Fize, C. Philouze, S. Demeshko, F. Meyer, M. Orio, V. Artero and C. Duboc, *ACS Catal.*, 2020, **10**, 177–186.
12 M. E. Ahmed, D. Saha, L. Wang, M. Gennari, S. Ghosh Dey, V. Artero, A. Dey and C. Duboc, *ChemElectroChem*, 2021, **8**, 1674–1677.
13 M. Gennari and C. Duboc, *Acc. Chem. Res.*, 2020, **53**, 2753–2761.
14 V. Artero and J.-M. Saveant, *Energy Environ. Sci.*, 2014, **7**, 3808–3814.
15 G.-G. Luo, H.-L. Zhang, Y.-W. Tao, Q.-Y. Wu, D. Tian and Q. Zhang, *Inorg. Chem. Front.*, 2019, **6**, 343–354.
16 N. Queyriaux, R. T. Jane, J. Massin, V. Artero and M. Chavarot-Kerlidou, *Coord. Chem. Rev.*, 2015, **304–305**, 3–19.
17 D. Dolui, S. Khandelwal, P. Majumder and A. Dutta, *Chem. Commun.*, 2020, **56**, 8166–8181.
18 A. R. Cutler and A. B. Todaro, *Organometallics*, 1988, **7**, 1782–1787.